Mineralogical Magazine, February 2015, Vol. 79(1), pp. 89–101

Fluor-tsilaisite, $NaMn_3Al_6(Si_6O_{18})(BO_3)_3(OH)_3F$, a new tourmaline from San Piero in Campo (Elba, Italy) and new data on tsilaisitic tourmaline from the holotype specimen locality

FERDINANDO BOSI[1,2,*], GIOVANNI B. ANDREOZZI[1,2], GIOVANNA AGROSI[3] AND EUGENIO SCANDALE[3]

[1] Dipartimento di Scienze della Terra, Sapienza Università di Roma, P. le Aldo Moro, 5, I-00185 Rome, Italy
[2] CNR- Istituto di Geoscienze e Georisorse, VOS Roma, P. le Aldo Moro, 5, I-00185 Rome, Italy
[3] Dipartimento di Scienze della Terra e Geoambientali, Università di Bari - Campus, via E. Orabona 4, I-70125 Bari, Italy

[*Received 30 April 2014; Accepted 10 July 2014; Associate Editor: S. Krivovichev*]

ABSTRACT

Fluor-tsilaisite, $NaMn_3Al_6(Si_6O_{18})(BO_3)_3(OH)_3F$, is a new mineral of the tourmaline supergroup. It occurs in an aplitic dyke of a LCT-type pegmatite body from Grotta d'Oggi, San Piero in Campo, Elba Island, Italy, in association with quartz, K-feldspar, plagioclase, elbaite, schorl, fluor-elbaite and tsilaisite. Crystals are greenish yellow with a vitreous lustre, sub-conchoidal fracture and white streak. Fluor-tsilaisite has a Mohs hardness of ~7 and a calculated density of 3.134 g/cm^3. In plane-polarized light, fluor-tsilaisite is pleochroic (O = pale greenish yellow and E = very pale greenish yellow), uniaxial negative. Fluor-tsilaisite is rhombohedral, space group *R*3*m*, a = 15.9398(6), c = 7.1363(3) Å, V = 1570.25(11) Å^3, Z = 3. The crystal structure of fluor-tsilaisite was refined to $R1$ = 3.36% using 3496 unique reflections collected with Mo$K\alpha$ X-ray intensity data. Crystal-chemical analysis resulted in the empirical formula: $^{X}(Na_{0.69}\square_{0.29}Ca_{0.02})_{\Sigma 1.00}{}^{Y}(Mn^{2+}_{1.29}Al_{1.21}Li_{0.56}Ti_{0.03})_{\Sigma 6.00}{}^{Z}Al_6{}^{T}(Si_{5.98}Al_{0.03})_{\Sigma 6.00}B_{2.92}O_{27}{}^{V}(OH)_3{}^{W}[F_{0.39}(OH)_{0.25}O_{0.36}]_{\Sigma 1.00}$.

Comparisons were performed between fluor-tsilaisite and a tsilaisitic tourmaline from the same locality as the holotype specimen. This latter tourmaline sample was selected for this study due to its remarkable composition (MnO = 11.63 wt.%), the largest Mn content found in tourmaline so far.

Fluor-tsilaisite is related to tsilaisite through the substitution $^{W}F \leftrightarrow {}^{W}(OH)$ and with fluor-elbaite through the substitution $^{Y}(Al + Li) \leftrightarrow 2{}^{Y}Mn^{2+}$, and appears to be a stepwise intermediate during tourmaline evolution from tsilaisite to fluor-elbaite.

KEYWORDS: fluor-tsilaisite, tourmaline, crystal-structure refinement, electron microprobe, new endmember.

Introduction

TOURMALINES are complex borosilicates and their crystal structure and crystal chemistry have been studied extensively (e.g. Foit, 1989; Hawthorne, 1996, 2002; Hawthorne and Henry, 1999; Andreozzi *et al*., 2008; Bosi, 2008, 2010, 2011, 2013; Lussier *et al*., 2008, 2011*a*,*b*; Novák *et al*., 2011; Henry and Dutrow, 2011; Filip *et al*., 2012; Skogby *et al*., 2012; Bosi *et al*., 2013*a*). In accordance with Henry *et al*. (2011), the general formula of tourmaline may be written as: $XY_3Z_6T_6O_{18}(BO_3)_3V_3W$, where X ($\equiv {}^{[9]}X$) = Na^+, K^+, Ca^{2+}, $\square$ (=vacancy); Y ($\equiv {}^{[6]}Y$) = Al^{3+}, Fe^{3+}, Cr^{3+}, V^{3+}, Mg^{2+}, Fe^{2+}, Mn^{2+}, Li^+; Z ($\equiv {}^{[6]}Z$) = Al^{3+}, Fe^{3+}, Cr^{3+}, V^{3+}, Mg^{2+}, Fe^{2+}; T ($\equiv {}^{[4]}T$) = Si^{4+}, Al^{3+}, B^{3+}; B ($\equiv {}^{[3]}B$) = B^{3+};

* E-mail: ferdinando.bosi@uniroma1.it
DOI: 10.1180/minmag.2015.079.1.08

W ($\equiv$ $^{[3]}$O1) = OH^{1-}, F^{1-}, O^{2-}; V ($\equiv$ $^{[3]}$O3) = OH^{1-}, O^{2-} and where, for example, T represents a group of cations (Si^{4+}, Al^{3+}, B^{3+}) accommodated at the [4]-coordinated *T* sites. The dominance of these ions at one or more sites of the structure gives rise to a range of distinct mineral species.

After the publication of the revised tourmaline classification (Henry *et al*., 2011), 14 new minerals of the tourmaline supergroup were approved by the Commission on New Minerals, Nomenclature and Classification (CNMNC) of the International Mineralogical Association (IMA): eight of these minerals are oxy-species, two are hydroxy-species and four are fluor-species (Table 1). Moreover, the aforementioned tourmaline classification allows reevaluation of samples previously studied. Actually, by reexamining different crystal fragments extracted from tourmalines previously studied from the island of Elba, Italy (Bosi *et al*., 2005; Agrosì *et al*., 2006), a new mineral, named tsilaisite (MnO = 9.60 wt.%) was found (Bosi *et al*., 2012*b*). Afterwards another fragment from the same macro-crystal, labeled Tsl2m (MnO = 9.19 wt.%), was found to be consistent with a new fluor-species, fluor-tsilaisite: $NaMn_3Al_6(Si_6O_{18})(BO_3)_3(OH)_3F$. The new mineral and its name have since been approved by the International Mineralogical Association Commission on New Minerals, Nomenclature and Classification (IMA 2012-044, Bosi *et al*., 2012*c*). The holotype specimen of fluor-tsilaisite is deposited in the collections of the "Museo di Scienze della Terra, settore Mineralogico Petrografico *Carlo Lorenzo Garavelli*", catalogue number NM16.

In this present study, the chemical, structural and physical properties of fluor-tsilaisite are discussed and compared with chemical and structural data of a new sample consistent with the root-composition of tsilaisite (CB1b) from the same locality as the holotype specimen (Grotta d'Oggi, San Piero in Campo, Elba Island, Italy). The tsilaisitic tourmaline, CB1b, was selected for this study due to its remarkable composition, representing the largest Mn content found in tourmaline so far, MnO = 11.63 wt.%.

Occurrence, appearance, physical and optical properties

The holotype fragment of fluor-tsilaisite (~0.4 mm × 0.4 mm × 0.3 mm in size) was

TABLE 1. New tourmalines approved by the IMA, after Henry *et al*. (2011).

Name	Endmember formula	Reference
Oxy-species		
Oxy-chromium-dravite	$NaCr_3(Cr_4Mg_2)(Si_6O_{18})(BO_3)_3(OH)_3O$	Bosi *et al*. (2012*a*)
Oxy-dravite	$NaAl_3(Al_4Mg_2)(Si_6O_{18})(BO_3)_3(OH)_3O$	Bosi and Skogby (2013)
Oxy-schorl	$Na(Fe_2Al)Al_6(Si_6O_{18})(BO_3)_3(OH)_3O$	Bačík *et al*. (2013)
Oxy-vanadium-dravite[a]	$NaV_3(V_4Mg_2)(Si_6O_{18})(BO_3)_3(OH)_3O$	Bosi *et al*. (2013*b*)
Darrellhenryite	$Na(LiAl_2)Al_6(Si_6O_{18})(BO_3)_3(OH)_3O$	Novák *et al*. (2013)
Vanadio-oxy-dravite	$NaV_3(Al_4Mg_2)(Si_6O_{18})(BO_3)_3(OH)_3O$	Bosi *et al*. (2014*a*)
Vanadio-oxy-chromium-dravite	$NaV_3(Cr_4Mg_2)(Si_6O_{18})(BO_3)_3(OH)_3O$	Bosi *et al*. (2014*b*)
Chromo-alumino-povondraite	$NaCr_3(Al_4Mg_2)(Si_6O_{18})(BO_3)_3(OH)_3O$	Reznitskii *et al*. (2014)
Hydroxy-species		
Tsilaisite	$NaMn_3Al_6(Si_6O_{18})(BO_3)_3(OH)_3(OH)$	Bosi *et al*. (2012*b*)
Adachiite	$CaFe_3Al_6(Si_5AlO_{18})(BO_3)_3(OH)_3(OH)$	Nishio-Hamane *et al*. (2013, 2014)
Fluor-species		
Fluor-dravite	$NaMg_3Al_6(Si_6O_{18})(BO_3)_3(OH)_3F$	Clark *et al*. (2011)
Fluor-schorl	$NaFe_3Al_6(Si_6O_{18})(BO_3)_3(OH)_3F$	Ertl *et al*. (2011)
Fluor-elbaite	$Na(Li_{1.5}Al_{1.5})Al_6(Si_6O_{18})(BO_3)_3(OH)_3F$	Bosi *et al*. (2013*c*)
Fluor-tsilaisite	$NaMn_3Al_6(Si_6O_{18})(BO_3)_3(OH)_3F$	This study

[a] Not a new mineral but the redefinition of "vanadium-dravite".

extracted from the basal region of the crystal from Grotta d'Oggi (Fig. 1). This crystal is a colour-zoned tourmaline ~9 mm long and 60 mm^2 in basal section. Its morphology consists of elongated {10$\bar{1}$0} and {11$\bar{2}$0} prisms terminated by a prominent {0001} pedion and small, minor {10$\bar{1}$1} pyramidal faces. Prism faces are striated (see fig. 1 in Bosi *et al*., 2012*b*). Fluor-tsilaisite occurs in an aplitic dyke of an LCT-type (lithium-, caesium- and tantalum-enriched) pegmatite body at Grotta d'Oggi, San Piero in Campo, Elba, Italy (Bosi *et al*. 2005; Agrosì *et al*., 2006), in association with quartz, K-feldspar, plagioclase, schorl, elbaite, fluor-elbaite and tsilaisite. Fluor-tsilaisite is greenish yellow with a vitreous lustre. It has a white streak and shows no fluorescence. Fluor-tsilaisite has a Mohs hardness of ~7 and is brittle with a {10$\bar{1}$1} and {11$\bar{2}$0} imperfect cleavage, {0001} parting and sub-conchoidal fracture inferred from the crystal. The calculated density is 3.134 g/cm^3. In transmitted light, fluor-tsilaisite is pleochroic with O = pale greenish yellow and E = very pale greenish yellow. Fluor-tsilaisite is uniaxial negative with refractive indices, measured by the immersion method using white light from a tungsten source, of ω = 1.645(5), ε = 1.625(5). The mean index of refraction, density and chemical composition lead to an excellent compatibility index ($1 - K_p/K_c$ = 0.035) (Mandarino, 1981). Similar to tsilaisite (Bosi *et al*., 2012*b*), the green-yellow colour of the fluor-tsilaisite can also be ascribed to an $Mn^{2+}-Ti^{4+}$ intervalence charge-transfer interaction which absorbs the violet-to-blue part of the visible spectrum (Rossman and Mattson, 1986).

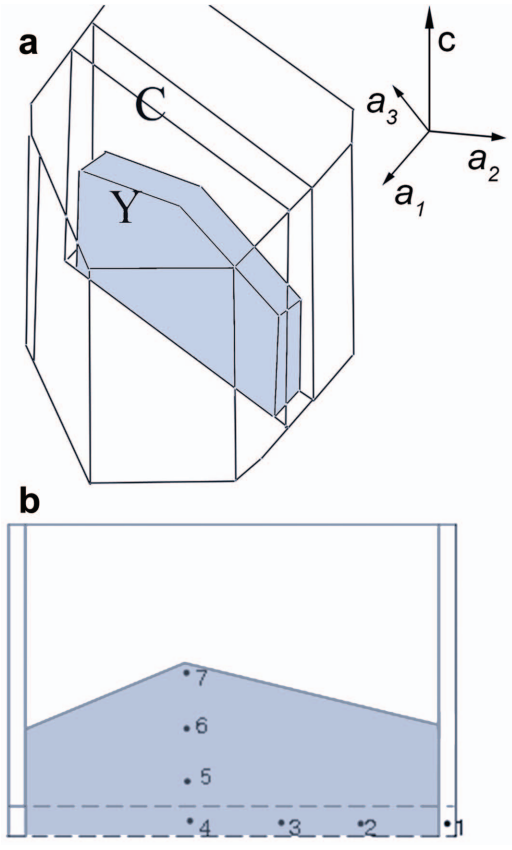

FIG. 1. Tourmaline crystal from Grotta d'Oggi: (*a*) Sketch of sample with the slice II2. C = colourless region, Y = greenish-yellow region (modified from Agrosì *et al*., 2006); (*b*) Sketch of the slice II2. Fluor-tsilaisite was extracted from the basal region of the slice II2. Crystal fragments characterized by SREF: 1 = fluor-elbaite; 2 = Mn-rich fluor-elbaite; 3 = fluor-tsilaisite (Tsl2m); 4 = tsilaisite; 5, 6, 7 = Mn-rich fluor-elbaite (modified from Bosi *et al*., 2005).

It should be noted that both tsilaisite (Bosi *et al*., 2012*b*) and fluor-tsilaisite come from the same crystal, which also includes fluor-elbaite (Fig. 1). Also, note that there is a typing mistake in the locality name in Bosi *et al*. (2012*b*): "San *Pietro* in Campo" should be "San *Piero* in Campo".

Experimental methods

Single-crystal structure refinement (SREF)

Structural data, collected on a single-crystal diffractometer equipped with a point detector, for the holotype fluor-tsilaisite were reported by Bosi *et al*. (2005) when describing sample Tsl2m.

A representative green-yellow crystal of tsilaisitic tourmaline (sample CB1b) was selected for X-ray diffraction (XRD) measurements on a Bruker KAPPA APEX-II single-crystal diffractometer (Sapienza University of Rome, Earth Sciences Department), equipped with a CCD area detector (6.2 cm × 6.2 cm active detection area, 512 × 512 pixels) and a graphite-crystal monochromator, using Mo$K\alpha$ radiation from a fine-focus sealed X-ray tube. The sample-to-detector distance was 4 cm. A total of 3681 exposures (step = 0.2º, time/step = 20 s) covering a full reciprocal sphere with a redundancy of ~14 was collected and a completeness of 99.7% was achieved. Final unit-cell parameters were refined using the Bruker AXS *SAINT* program on

reflections with $I > 10\sigma(I)$ in the range $5^{o} < 2\theta < 72^{o}$. The intensity data were processed and corrected for Lorentz, polarization and background effects with the *APEX2* software program of Bruker AXS. The data were corrected for absorption using a multi-scan method (*SADABS*). The absorption correction led to a significant improvement in R_{int}. No violations of *R*3*m* symmetry were noted.

Structure refinement was undertaken with the *SHELXL-2013* program (Sheldrick, 2013). Starting coordinates were taken from Bosi *et al*. (2010). Variable parameters were: scale factor, extinction coefficient, atom coordinates, site-scattering values expressed as mean atomic number (for *X*, *Y* and *Z* sites) and atomic-displacement factors. A first refinement was performed modelling the *X* site by the Na scattering factor, the *Y* site by considering the presence of Mn *vs*. Li and the *Z* site by Al. The *T*, *B* and anion sites were modelled, respectively, with Si, B and O scattering factors and with a fixed occupancy of 1. With this structure model, convergence was achieved rapidly and the variance-covariance matrix showed no significant correlations between the refined parameters. The results showed mean atomic numbers for *X*, *Y* and *Z* of 7.0(1), 17.9(1) and 13.4(1), respectively, with disagreement indices *R*1 (for all reflections) and *wR*2 of 0.0166 and 0.0397, respectively. A further refinement with chemical constraints was then carried out by modelling the site occupancy as follows: the *X* site, by Na with the occupancy of Ca and K fixed to the value obtained from the structural formula; the *Y* site, by Mn *vs*. Al and with the occupancy of Li, Fe and Ti fixed to the value of the structural formula; the Z site, by Al *vs*. Mn; the O1 site with occupancy of O and F fixed to the value of the structural formula. The results are practically equal to those obtained for the first refinement. Following the findings of Burns *et al*. (1994) who reported high U_{eq} values for the O1 and O2 sites that indicate position disorder, the crystal was refined twice: (1) with both sites constrained to their positions of maximum site-symmetry, (00*z*) for O1 and (*x*, 1−*x*, *z*) for O2; and (2) with both sites allowed to disorder with coordinates

TABLE 2. Single-crystal XRD data for fluor-tsilaisite and sample CB1b.

Sample	Tsl2m (data from Bosi *et al*., 2005)	CB1b
Crystal size (mm)	0.25 × 0.27 × 0.31	0.20 × 0.22 × 0.26
a (Å)	15.9398(6)	15.9619(4)
c (Å)	7.1363(3)	7.1426(2)
V (Å^3)	1570.3(1)	1576.71(9)
Range for data collection, 2θ (º)	5−95	5−73
Reciprocal space range, *hkl*	$0 \leqslant h \leqslant 28$	$-26 \leqslant h \leqslant 26$
	$0 \leqslant k \leqslant 28$	$-26 \leqslant k \leqslant 26$
	$-14 \leqslant l \leqslant 14$	$-11 \leqslant l \leqslant 10$
Set of measured reflections	3496	13,288
Unique reflections, R_{int} (%)	3496	1746, 2.59
Absorption correction method	Semi-empirical, 13 ψ scans	SADABS
Refinement method	Full-matrix last-squares on F^2	Full-matrix last-squares on F^2
Structural refinement program	*SHELXL-97*	*SHELXL-2013*
Extinction coefficient	0.00173(5)	0.0057(3)[a], 0.0056(3)[b]
Flack parameter	0.14(2)	0.02(3)[a], 0.03(2)[b]
*wR*2 (%)	7.76	3.93[a], 3.68[b]
*R*1 (%) all data	3.86	1.66[a], 1.54[b]
*R*1 (%) for $I > 2\sigma(I)$	3.36	1.64[a], 1.52[b]

R_{int} = merging residual value; *R*1 = discrepancy index, calculated from *F*-data; *wR*2 = weighted discrepancy index, calculated from F^2-data; Radiation, Mo*K*α = 0.71073 Å. Data collection temperature = 293 K. Space group *R*3*m*; *Z* = 3.
[a] Standard SREF denotes structural refinement undertaken with O1 at (0,0,*z*) and O2 at (*x*,2*x*,*z*).
[b] Split-site SREF denotes structural refinement undertaken with O1 at (*x*,2*x*,*z*) and O2 at (*x*,*y*,*z*) to allow for positional disorder, as indicated by the high U_{eq} values (Burns *et al*., 1994).

(x, $x/2$, z) and (x,y,z) (referred to as split-site SREF in this study). There were no correlations >0.7 between the parameters at the end of the refinement. Table 2 lists crystal data, data-collection information and refinement details. Fractional atom coordinates and equivalent isotropic-displacement parameters are reported in Table 3; anisotropic-displacement parameters in Table 4; and selected bond lengths in Table 5. For comparison, the data for sample Tsl2m are also reported. A crystallographic information file has been deposited with the Principal Editor of *Mineralogical Magazine* and is available from www.minersoc.org/pages/e_journals/dep_mat_mm.html.

Microprobe analysis

Chemical data, obtained by electron microprobe and secondary-ion mass spectrometry (SIMS), for the holotype fluor-tsilaisite were reported by Bosi *et al*. (2005) when describing sample Tsl2m.

Electron-microprobe analyses for sample CB1b were obtained by wavelength-dispersive spectrometer (WDS mode) with a Cameca SX50 instrument at the "Istituto di Geologia Ambientale e Geoingegneria (Rome, Italy), CNR", operating at an accelerating potential of 15 kV and a sample current of 15 nA, 10 μm beam diameter. Minerals and synthetic compounds were used as standards: wollastonite

TABLE 3. Fractional atom coordinates and site occupancy for sample CB1b.

Site	x	y	z	Site occupancy
Standard SREF				
X	0	0	0.2257(5)	$Na_{0.614(11)}$ $Ca_{0.0143}$ $K_{0.0046}$
Y	0.12432(4)	0.06216(2)	0.62286(10)	$Mn_{0.481(6)}$ $Al_{0.395(6)}$ $Li_{0.1019}$ $Ti_{0.0137}$ $Fe_{0.009}$
Z	0.29816(3)	0.26145(3)	0.61080(9)	$Al_{0.969(4)}$ $Mn_{0.031(4)}$
B	0.11012(8)	0.22025(16)	0.4541(3)	$B_{1.00}$
T	0.19185(3)	0.18988(3)	0	$Si_{0.9895}$ $Al_{0.0105}$
O1	0	0	0.7780(6)	$O_{0.6537}$ $F_{0.3463}$
O2	0.06157(6)	0.12315(13)	0.4827(3)	$O_{1.00}$
O3	0.26844(14)	0.13422(7)	0.5098(3)	$O_{1.00}$
O4	0.09366(6)	0.18732(12)	0.0693(2)	$O_{1.00}$
O5	0.18713(12)	0.09357(6)	0.0913(2)	$O_{1.00}$
O6	0.19745(8)	0.18725(8)	0.77534(18)	$O_{1.00}$
O7	0.28527(7)	0.28572(7)	0.07944(17)	$O_{1.00}$
O8	0.20999(8)	0.27099(8)	0.44110(18)	$O_{1.00}$
H3	0.260(3)	0.1301(14)	0.394(6)	$H_{1.00}$
Split-site SREF				
X	0	0	0.2263(5)	$Na_{0.609(10)}$ $Ca_{0.0143}$ $K_{0.0046}$
Y	0.12435(3)	0.06218(2)	0.62283(9)	$Mn_{0.489(5)}$ $Al_{0.387(5)}$ $Li_{0.1019}$ $Ti_{0.0137}$ $Fe_{0.009}$
Z	0.29815(3)	0.26144(3)	0.61085(8)	$Al_{0.969(3)}$ $Mn_{0.031(3)}$
B	0.11012(8)	0.22024(15)	0.4541(3)	$B_{1.00}$
T	0.19184(2)	0.18987(3)	0	$Si_{0.9895}$ $Al_{0.0105}$
O1	0.0199(3)	0.00995(13)	0.7783(5)	$O_{0.6537}$ $F_{0.3463}$
O2	0.07173(15)	0.12324(12)	0.4828(3)	$O_{1.00}$
O3	0.26855(13)	0.13428(7)	0.5098(2)	$O_{1.00}$
O4	0.09362(5)	0.18724(11)	0.0692(2)	$O_{1.00}$
O5	0.18711(11)	0.09355(6)	0.0913(2)	$O_{1.00}$
O6	0.19741(7)	0.18721(7)	0.77540(17)	$O_{1.00}$
O7	0.28525(7)	0.28572(7)	0.07943(16)	$O_{1.00}$
O8	0.20996(7)	0.27103(7)	0.44122(17)	$O_{1.00}$
H3	0.259(3)	0.1295(13)	0.400(5)	$H_{1.00}$

Standard and split-site SREF denote, respectively, structural refinements carried out with the O1 site at (0,0,z) and the O2 site at (x,2x,z), and with O1 at (x,x/2,z) and O2 at (x,y,z) to allow for positional disorder, as indicated by the high U_{eq} values (Burns *et al*., 1994).

TABLE 4. Displacement parameters (Å^2) for sample CB1b.

Site	U^{11}	U^{22}	U^{33}	U^{23}	U^{13}	U^{12}	U_{eq}/U_{iso}*
Standard SREF							
X	0.0288(13)	0.0288(13)	0.0233(19)	0	0	0.0144(6)	0.0269(11)
Y	0.0101(2)	0.00757(17)	0.0182(3)	−0.00157(8)	−0.00314(16)	0.00507(11)	0.01170(15)
Z	0.00643(19)	0.00703(19)	0.0054(2)	0.00056(14)	−0.00012(13)	0.00342(14)	0.00625(13)
B	0.0074(6)	0.0057(8)	0.0067(9)	0.0000(6)	0.0000(3)	0.0029(4)	0.0068(3)
T	0.00481(16)	0.00467(15)	0.00484(18)	−0.00042(12)	−0.00017(12)	0.00239(11)	0.00476(9)
O1	0.062(2)	0.062(2)	0.0083(18)	0	0	0.0310(10)	0.0441(12)
O2	0.0318(9)	0.0054(6)	0.0131(10)	0.0005(6)	0.0003(3)	0.0027(3)	0.0197(4)
O3	0.0249(8)	0.0111(5)	0.0050(7)	−0.0002(3)	−0.0003(6)	0.0124(4)	0.0121(3)
O4	0.0065(4)	0.0129(7)	0.0081(7)	−0.0013(5)	−0.0007(3)	0.0064(3)	0.0084(3)
O5	0.0140(7)	0.0068(4)	0.0080(7)	0.0008(3)	0.0017(5)	0.0070(3)	0.0088(3)
O6	0.0084(4)	0.0096(4)	0.0044(5)	−0.0004(3)	0.0002(3)	0.0040(3)	0.00769(19)
O7	0.0059(4)	0.0060(4)	0.0056(5)	−0.0007(3)	−0.0001(3)	0.0015(3)	0.00650(18)
O8	0.0058(4)	0.0116(5)	0.0082(5)	0.0029(4)	0.0007(3)	0.0052(4)	0.00816(19)
H3							0.018*
Split-site SREF							
X	0.0277(12)	0.0277(12)	0.0228(17)	0	0	0.0138(6)	0.0260(10)
Y	0.0101(2)	0.00761(15)	0.0185(3)	−0.00157(7)	−0.00315(15)	0.00507(10)	0.01182(14)
Z	0.00649(18)	0.00700(18)	0.0052(2)	0.00057(13)	−0.00014(12)	0.00346(13)	0.00620(12)
B	0.0077(5)	0.0066(7)	0.0063(9)	0.0000(6)	0.0000(3)	0.0033(4)	0.0070(3)
T	0.00463(14)	0.00463(14)	0.00482(16)	−0.00042(11)	−0.00012(11)	0.00236(10)	0.00467(8)
O1							0.0121(10)*
O2							0.0086(4)*
O3	0.0244(8)	0.0110(4)	0.0048(7)	−0.0001(3)	−0.0003(5)	0.0122(4)	0.0119(3)
O4	0.0064(4)	0.0123(6)	0.0082(6)	−0.0013(5)	−0.0006(2)	0.0062(3)	0.0083(2)
O5	0.0141(6)	0.0066(4)	0.0079(7)	0.0006(2)	0.0012(5)	0.0070(3)	0.0087(2)
O6	0.0083(4)	0.0097(4)	0.0041(4)	−0.0006(3)	−0.0001(3)	0.0039(3)	0.00763(17)
O7	0.0057(3)	0.0058(3)	0.0057(4)	−0.0008(3)	−0.0001(3)	0.0014(3)	0.00643(17)
O8	0.0057(4)	0.0117(4)	0.0079(5)	0.0028(3)	0.0008(3)	0.0052(3)	0.00808(18)
H3							0.018*

* Equivalent (U_{eq}) and isotropic (U_{iso}) displacement parameters; the H atom was constrained to have a U_{iso} 1.5 times the U_{eq} value of the O3 oxygen. Standard and split-site SREF denote, respectively, structural refinements carried out with the O1 site at (0,0,z) and the O2 site at (*x*,2*x*,*z*), and with O1 at (*x*,*x*/2,*z*) and O2 at (*x*,*y*,*z*) to allow for positional disorder, as indicated by the high U_{eq} values (Burns *et al*., 1994).

(Si, Ca), magnetite (Fe), rutile (Ti), corundum (Al), vanadinite (V) fluorphlogopite (F), periclase (Mg), jadeite (Na), K-feldspar (K), sphalerite (Zn), metallic Cr, Mn and Cu. The "*PAP*" routine was applied (Pouchou and Pichoir, 1991). The results (Table 6) represent mean values of ten spot analyses. Vanadium, Cr, Zn and Cu were below their respective detection limits (0.03 wt.%) in the sample studied.

Powder X-ray diffraction

Powder XRD data for sample Tsl2m were derived from the single-crystal structural refinement as there was not enough material available for powder-diffraction measurements. However, the data were considered unsuitable for diagnostic identification of fluor-tsilaisite and they are not given here.

Results and discussion

Determination of atom proportions

In agreement with the structure-refinement results, the boron content was assumed to be stoichiometric in sample CB1b (B^{3+} = 3.00 atoms per formula unit, a.p.f.u.). Both the site-scattering results and the bond lengths of *B* and *T* are

TABLE 5. Selected bond lengths (Å) for fluor-tsilaisite and sample CB1b.

	Tsl2m	CB1b		
		Standard SREF		Split-site SREF
X–O2 (×3)	2.478(3)	2.503(3)		2.507(3)
X–O5 (×3)	2.7617(17)	2.759(2)		2.7604(19)
X–O4 (×3)	2.8218(17)	2.820(2)		2.821(2)
<*X*–O>	2.687	2.694		2.696
Y–O2 (×2)	1.9794(11)	1.9823(13)	*Y*–O1	1.822(4)
Y–O6 (×2)	2.037(2)	2.045(2)	*Y*–O2 (×2)	1.865(2)
Y–O1	2.0453(9)	2.0508(12)	*Y*–O6 (×2)	2.0508(11)
Y–O3	2.1641(17)	2.150(2)	*Y*–O2 (×2)	2.107(2)
<*Y*–O>	2.042	2.044	*Y*–O3	2.1505(18)
			Y–O1 (×2)	2.177(3)
Z–O6	1.8577(9)	1.8613(12)		1.8617(11)
Z–O7	1.8789(8)	1.8817(12)		1.8820(11)
Z–O8	1.8812(9)	1.8837(12)		1.8840(11)
Z–O8′	1.9168(9)	1.9204(12)		1.9206(11)
Z–O7	1.9554(8)	1.9588(11)		1.9590(10)
Z–O3	1.9731(7)	1.9773(9)		1.9769(8)
<*Z*–O>	1.911	1.914		1.914
B–O2	1.356(2)	1.358(3)		1.366(3)
B–O8 (×2)	1.3860(12)	1.3836(16)		1.3832(15)
<*B*–O>	1.376	1.375		1.377
T–O6	1.6058(8)	1.6089(13)		1.6084(12)
T–O7	1.6156(8)	1.6142(11)		1.6141(10)
T–O4	1.6237(5)	1.6244(7)		1.6244(6)
T–O5	1.6375(6)	1.6373(8)		1.6371(7)
<*T*–O>	1.621	1.621		1.621

For sample Tsl2m, bond lengths are derived from the fractional atom coordinates of Bosi *et al*. (2005). Standard and split-site SREF denote, respectively, structural refinements carried out with the O1 site at (0,0,*z*) and the O2 site at (*x*,2*x*,*z*), and with O1 at (*x*,*x*/2,*z*) and O2 at (*x*,*y*,*z*) to allow for positional disorder, as indicated by the high U_{eq} values (Burns *et al*., 1994).

consistent with the *B* site fully occupied by boron and no B^{3+} at the *T* site (e.g. Hawthorne, 1996; Bosi and Lucchesi, 2007). As polarized optical spectra showed no Mn^{3+} absorption bands for Mn-rich tourmaline and tsilaisite fragments extracted from the crystal from Grotta d'Oggi (Bosi *et al*., 2012b), it is concluded that Mn occurs only in the divalent state in sample CB1b. The small amounts of Fe were calculated as Fe^{2+}. The (OH) content was obtained as a result of the equation of Bosi (2013): ^{W}(OH) = [2 − 1.01 BVS(O1) − 0.21 − F]. As the experimental bond-valence sum (BVS) at the O1 site is 1.13 valence units (bond-valence parameters from Brown and Altermatt, 1985), the resulting (OH) content is 3.30 a.p.f.u. The Li content can then be calculated by charge balance with the assumption *T* + *Y* + *Z* = 15.00. The atomic proportions were calculated on this assumption (Table 6). The validity of this procedure is further confirmed by the excellent convergence at 240.5 of the number of electrons per formula unit derived from both chemical and structural (split-site SREF) approaches.

Site populations

The anion site populations in the sample studied follow the general preference suggested for tourmaline (e.g. Grice and Ercit, 1993; Henry *et al*., 2011): the O3 site (V position in the general formula) is occupied by $(OH)^{1-}$ and the O1 site

TABLE 6. Chemical composition of fluor-tsilaisite and sample CB1b.

	Tsl2m (from Bosi *et al*., 2005)	CB1b
SiO_2 (wt.%)	36.16(9)	35.65(14)
TiO_2	0.27(7)	0.33(8)
B_2O_3	10.22(56)[a]	10.44[c]
Al_2O_3	37.15(20)	35.92(16)
MnO	9.19(7)[b]	11.63(20)[b]
FeO	b.d.l.	0.19(6)[b]
CaO	0.14(2)	0.08(2)
Na_2O	2.14(10)	1.92(4)
K_2O	0.02(1)	0.02(1)
Li_2O	0.85(10)[a]	0.46[c]
F	0.74(10)	0.66(9)
H_2O	2.95(16)[a]	2.97[d]
-O=F	−0.31	−0.28
Total	99.52	100.00
Si (a.p.f.u.)	5.98	5.94
Ti^{4+}	0.03	0.04
B	2.92	3.00
Al	7.21	7.05
Mn^{2+}	1.29	1.64
Fe^{2+}	–	0.03
Ca	0.02	0.01
Na	0.69	0.62
K	0.003	0.005
Li	0.56	0.31
F	0.39	0.35
OH	3.25	3.30

[a] Measured by secondary-ion mass spectrometry
[b] Calculated as divalent cation (see text).
[c] Calculated by stoichiometry
[d] Calculated by crystal chemical constraints (see text).
Errors for oxides are standard deviations (in brackets) of 10 spot analyses; b.d.l. = below detection limits, a.p.f.u. = atoms per formula unit.

(W position in the general formula) is occupied by O^{2-}, $(OH)^{1-}$ and F^{1-}. Also, the *X* site population follows the general preference suggested for tourmaline with the amounts of Na, Ca and K in line with the observed *X* mean atomic number. The cation distribution at the *T* site ($Si_{5.94}Al_{0.06}$) was obtained by accommodating all Si^{4+} (5.94 a.p.f.u.) plus amounts of Al^{3+} (0.06 a.p.f.u.) to have 6 a.p.f.u. The mean bond distance <*T*–O> derived from this population is in excellent agreement with the data of MacDonald and Hawthorne (1995): <*T*–O> = (1.620 + 0.0162 $^{[4]}$Al). The site populations over the *Y* and *Z* sites were obtained by assuming Li^{1+} and very small concentrations of Fe^{2+} and Ti^{4+} at the *Y* site (Henry *et al*., 2011), and then optimizing (using a quadratic program) the amounts of Al and Mn over *Y* and *Z* according to the observed mean atomic numbers (Table 7).

The final empirical formula for sample CB1b is as follows:

$^{X}(Na_{0.62}\square_{0.36}Ca_{0.01}K_{0.005})_{\Sigma 1.00}$
$^{Y}(Mn^{2+}_{1.45}Al_{1.17}Li_{0.31}Ti_{0.04}Fe^{2+}_{0.03})_{\Sigma 3.00}$
$^{Z}(Al_{5.81}Mn^{2+}_{0.19})_{\Sigma 6.00}[^{T}(Si_{5.94}Al_{0.06})O_{18}]^{B}(BO_3)_3$
$^{V}(OH)_3{}^{W}[F_{0.35}O_{0.35}(OH)_{0.30}]_{\Sigma 1.00}$.

This formula is also consistent with that obtained by the procedure of Wright *et al*. (2000), assuming the default setting but with the chemical variability constrained by electroneutrality (Table 7).

For comparison, the empirical formula of the holotype sample Tsl2m, rearranged with appropriate grouping of constituents (Bosi *et al*., 2012*c*), is:

$^{X}(Na_{0.69}\square_{0.29}Ca_{0.02})_{\Sigma 1.00}$
$^{Y}(Mn^{2+}_{1.29}Al_{1.21}Li_{0.56}Ti_{0.03})_{\Sigma 3.00}{}^{Z}Al_6$
$^{T}(Si_{5.98}Al_{0.03})_{\Sigma 6.00}B_{2.92}O_{27}{}^{V}(OH)_3{}^{W}[F_{0.39}(OH)_{0.25}O_{0.36}]_{\Sigma 1.00}$.

Name and crystal chemistry

Tourmaline sample Tsl2m is a new species in accord with the recommendations of Henry *et al*. (2011). The empirical formula of Tsl2m shows that the content of $^{Y}Mn^{2+}$ (= 1.29 a.p.f.u.) is larger than 2^{Y}Li (= 1.12 a.p.f.u.), typical of a ^{X}Na-, ^{Z}Al-dominant tourmaline belonging to the alkali-subgroup 2. The amount of monovalent anions at the W position (F + OH = 0.64 a.p.f.u.) is larger than that of divalent anions (O^{2-} = 0.36 a.p.f.u.). Consequently, in accordance with the dominant-valence rule (e.g. Henry *et al*., 2011), the dominant anion of the dominant valence at one site becomes the basis for naming the species. As F (= 0.39 a.p.f.u.) is larger than OH (= 0.25 a.p.f.u.), this tourmaline is named fluor-tsilaisite. This species, ideally $NaMn_3Al_6(Si_6O_{18})(BO_3)_3(OH)_3F$, can be derived from the root composition of tsilaisite, $NaMn_3Al_6(Si_6O_{18})(BO_3)_3(OH)_3OH$, *via* the substitution F → (OH) at the W position of the general formula.

It is worth noting that the (OH) content of sample Tsl2m was measured by SIMS, and thus there is direct experimental evidence for $^{W}F > {}^{W}$(OH), whereas that of sample CB1b has been

TABLE 7. Cation site populations (a.p.f.u.) and mean atomic numbers for sample CB1b.

Site	Site population	Mean atomic number		
		Calculated	Standard SREF	Split-site SREF
X	0.62 Na + 0.36 □ + 0.01 Ca + 0.005 K	7.23	7.13(8)	7.07(7)
Y	1.45 Mn^{2+} + 1.17 Al + 0.31 Li + 0.04 Ti + 0.03 Fe^{2+}	18.04	18.0(1)	18.09(9)
	(1.43 Mn^{2+} + 1.20 Al + 0.30 Li + 0.03 Ti + 0.04 Fe^{2+})[a]			
Z	5.81 Al + 0.19 Mn^{2+}	13.37	13.37(5)	13.38(5)
	^{Z}(5.80 Al + 0.20 Mn^{2+})[a]			
T	5.94 Si + 0.06 Al	13.99	13.99[b]	13.99[b]
B	3 B	5	5[b]	5[b]

Standard and split-site SREF denote, respectively, structural refinements carried out with the O1 site at (0,0,*z*) and the O2 site at (*x*,2*x*,*z*), and with O1 at (*x*,*x*/2,*z*) and O2 at (*x*,*y*,*z*) to allow for positional disorder, as indicated by the high U_{eq} values (Burns *et al.* 1994). a.p.f.u. = atoms per formula unit.

[a] Site populations optimized by the procedure of Wright *et al.* (2000).

[b] Fixed in the final stages of refinement

inferred by crystal-chemical considerations. Because the F and (OH) contents are quite similar in sample CB1b [0.35 a.p.f.u. F and 0.30 a.p.f.u. (OH)], there is some uncertainty in naming this tsilaisitic tourmaline as fluor-tsilaisite or tsilaisite. Apart from the name, the bulk composition of this sample is very interesting as it is in contrast to the predictions summarized by London (2011) about the limitation of Mn substitution into tourmaline solid-solutions at ~1.5 a.p.f.u. In fact, sample CB1b is the most Mn^{2+}-rich tourmaline found in Nature so far: Mn^{2+} = 1.64 a.p.f.u. Other Mn^{2+}-rich tourmalines showing Mn^{2+} amounts consistent with the root-composition of tsilaisite and characterized by SREF are reported in Table 8. The plot of these compositions in the ternary diagram for 2Li–Fe^{2+}–Mn^{2+} is displayed in Fig. 2.

In accord with the crystal-structure information, Bosi *et al*. (2005) suggested that limited disorder of Al and Mn^{2+} over the *Y* and *Z* sites might occur in Mn-rich tourmaline. On the other hand, Ertl *et al*. (2012) suggested complete ordering of Mn^{2+} at the *Y* site, ascribing the relatively large value of <Z–O> to inductive effects. Bosi and Andreozzi (2013) summarized all previous studies on Mn-rich tourmalines and ruled out inductive effects of $^{Y}Mn^{2+}$ on <Z–O>, concluding that there is no solid evidence for the occurrence of Mn^{2+} at *Z*. The observed <Z–O> variations in Mn-bearing tourmalines (1.902–1.911 Å) are consistent with <*Z*–O> variation observed in 110 tourmalines having the *Z* site fully occupied by Al (1.900–1.912 Å). For sample CB1b, the observed <Z–O> is 1.914 Å, which is out of this typical

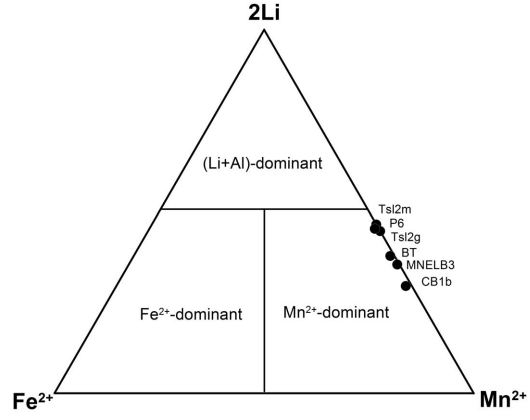

FIG. 2. Ternary diagram 2Li–Fe^{2+}–Mn^{2+} for tourmalines with root composition of tsilaisite characterized by SREF (see Table 8 for details).

TABLE 8. Tourmalines with root composition of tsilaisite.

Sample	MnO (wt.%)	Mn (a.p.f.u.)	Provenance	Reference
CB1b	11.63	1.64	Grotta d'Oggi, San Piero in Campo, Elba Island, Italy	This study
Tsl2g	9.60	1.34	Grotta d'Oggi, San Piero in Campo, Elba Island, Italy	Bosi *et al*. (2012*b*)
MNELB3	9.28	1.30	Fosso dei Forcioni, Sant'Ilario in Campo, Elba Island, Italy	Ertl *et al*. (2012)
Tsl2m	9.18	1.29	Grotta d'Oggi, San Piero in Campo, Elba Island, Italy	Bosi *et al*. (2005)
BT	8.86	1.23	Eibenstein an der Thaya, Lower Austria	Ertl *et al*. (2003)
P6	8.18	1.14	Eibenstein an der Thaya, Lower Austria	Ertl *et al*. (2003)

<*Z*–O> range for samples with the *Z* site fully occupied by Al and may be consistent with the occurrence of cations larger than Al at the *Z* site (i.e. Mn^{2+}). Moreover, the observed *Z* mean atomic number of sample CB1b, 13.4(1), is significantly larger than the value of 13 expected for a *Z* site fully occupied by Al, and is consistent with the occurrence of cations heavier than Al at the *Z* site (i.e. Mn^{2+}). This result indicates that $^{Y}Al + {}^{Z}Mn^{2+} \rightarrow {}^{Y}Mn^{2+} + {}^{Z}Al$ disorder (up to 0.20 a.p.f.u.) may occur in sample CB1b, as shown by the optimization results (Table 7). On this basis and according to the structural information reported by Bosi *et al*. (2005), some degree of disorder of Al and Mn^{2+} over *Y* and *Z* is also considered possible for sample Tsl2m, leading to the following disordered formula for the fluor-tsilaisite holotype specimen:

$^{X}(Na_{0.69}\square_{0.29}Ca_{0.02})_{\Sigma 1.00}$
$^{Y}(Mn^{2+}_{1.19}Al_{1.31}Li_{0.56}Ti_{0.03})_{\Sigma 3.00}{}^{Z}(Al_{5.90}Mn^{2+}_{0.10})_{\Sigma 6.00}$
$^{T}(Si_{5.98}Al_{0.03})_{\Sigma 6.00}B_{2.92}O_{27}{}^{V}(OH)_{3}$
$^{W}[F_{0.39}(OH)_{0.25}O_{0.36}]_{\Sigma 1.00}$.

Relation to other species

Comparative data for fluor-tsilaisite, tsilaisite and fluor-elbaite are given in Table 9. On the basis of available information, fluor-tsilaisite and tsilaisite may be distinguished only by detailed chemical characterization, because of their similar physical and optical properties.

TABLE 9. Comparative data for fluor-tsilaisite, tsilaisite and fluor-elbaite.

	Fluor-tsilaisite	Tsilaisite	Fluor-elbaite
a (Å)	15.9398(6)	15.9461(5)	15.8933(2)
c (Å)	7.1363(3)	7.1380(3)	7.1222(1)
V (Å^3)	1570.3(1)	1571.9(1)	1558.02(4)
Space group	*R*3*m*	*R*3*m*	*R*3*m*
Optic sign	Uniaxial (−)	Uniaxial (−)	Uniaxial (−)
ω	1.645(5)	1.645(5)	1.640(5)
ε	1.625(5)	1.625(5)	1.625(5)
Streak	White	White	White
Colour	Greenish yellow	Greenish yellow	Blue green
Pleochroism	O = pale greenish E = very pale greenish	O = pale greenish E = very pale greenish	O = green E = pale green
Y population	$Mn^{2+}_{1.3}Al_{1.2}Li_{0.6}$	$Mn^{2+}_{1.3}Al_{1.1}Li_{0.5}$	$Al_{1.2}Li_{1.0}Fe^{2+}_{0.5}Mn^{2+}_{0.3}$
W population	$F_{0.4}(OH)_{0.25}O_{0.36}$	$F_{0.4}(OH)_{0.4}O_{0.2}$	$F_{0.8}(OH)_{0.2}$
Reference	Bosi *et al*. (2005)	Bosi *et al*. (2012*b*)	Bosi *et al*. (2013*c*)

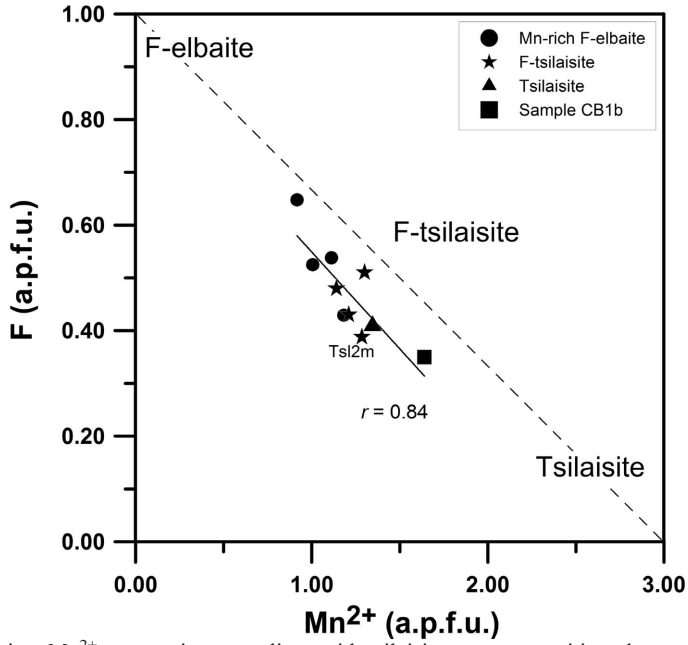

FIG. 3. Plot of F against Mn^{2+} content in tourmalines with tsilaisite root composition characterized by SREF (see references in Table 8). Four Mn-rich fluor-elbaite samples belonging to the crystal of the holotype were added (data from Bosi *et al*., 2005). The black line indicates the linear fit F = (0.92 − 0.37 Mn) with coefficients very close to those of the ideal relationship, dashed line, F = (1 − 0.33 Mn). Modified from Bosi *et al*. (2012*b*).

Fluor-tsilaisite is related to tsilaisite through the substitution $^{W}F \leftrightarrow {}^{W}(OH)$ and with fluor-elbaite through the substitution $^{Y}(Al + Li) \leftrightarrow 2{}^{Y}Mn^{2+}$. Ideally, fluor-tsilaisite may be linked to elbaite through the substitution $2{}^{Y}Mn^{2+} + {}^{W}F \leftrightarrow {}^{Y}(Al + Li) + {}^{W}(OH)$, but Bosi *et al*. (2012*b*) observed an inverse correlation between F and Mn^{2+} that makes compositions intermediate between fluor-tsilaisite and ebaite unlikely. The plot of F against Mn^{2+} shows that samples Tsl2m and CB1b are consistent with such an inverse correlation, ideally F = 1 − 0.33 Mn (a.p.f.u.), confirming the absence of solid solution between fluor-tsilaisite and elbaite (Fig. 3). In the core-to-rim chemical evolution of the zoned crystal from Grotta d'Oggi, the fluor-tsilaisite appears to be a stepwise intermediate composition from the tsilaisitic core to the fluor-elbaite rim (Fig. 1). The whole process is described ideally by the substitution $^{Y}(Al + Li) + {}^{W}F \leftrightarrow 2{}^{Y}Mn^{2+} + {}^{W}(OH)$.

Implications

The discovery of the new mineral fluor-tsilaisite further expands the compositional field and the crystal-chemical variability of the tourmaline supergroup. The existence and possibility of crystallization of fluor-tsilaisite should therefore be considered when exploring the tourmaline solid-solutions obtained by mixing Li^{+}, Mn^{2+} and Al^{3+} with F^{1-}, $(OH)^{1-}$ and O^{2-}. Furthermore, the present study has shown that tsilaisite, fluor-tsilaisite and fluor-elbaite are closely related and can occur in the same tourmaline crystal, even where the crystal size is <10 mm (Fig. 1). This suggests that other new tourmalines may occur in zoned crystals in which the chemical evolution may mirror the evolution of the host environment.

Acknowledgements

Chemical analyses were performed with the kind assistance of M. Serracino to whom the authors express their gratitude. The reviews of Frank C. Hawthorne and an anonymous reveiwer and the editorial handling of Sergey V. Krivovichev are acknowledged.

References

Agrosì, G., Bosi, F., Lucchesi, S., Melchiorre, G. and Scandale, E. (2006) Mn-tourmaline crystals from

island of Elba (Italy): Growth history and growth marks. *American Mineralogist*, **91**, 944–952.

Andreozzi, G.B., Bosi, F. and Longo, M. (2008) Linking Mössbauer and structural parameters in elbaite-schorl-dravite tourmalines. *American Mineralogist*, **93**, 658–666.

Bačík, P., Cempírek, J., Uher, P., Novák, M., Ozdín, D., Filip, J., Škoda, R., Breiter, K., Klementová, M. and Ďud'a, R. (2013) Oxy-schorl, $Na(Fe^{2+}_2Al)Al_6Si_6O_{18}(BO_3)_3(OH)_3O$, a new mineral from Zlatá Idka, Slovak Republic and Přibyslavice, Czech Republic. *American Mineralogist*, **98**, 485–492,

Bosi, F. (2008) Disordering of Fe^{2+} over octahedrally coordinated sites of tourmaline. *American Mineralogist*, **93**, 1647–1653.

Bosi, F. (2010) Octahedrally coordinated vacancies in tourmaline: a theoretical approach. *Mineralogical Magazine*, **74**, 1037–1044.

Bosi, F. (2011) Stereochemical constraints in tourmaline: from a short-range to a long-range structure. *The Canadian Mineralogist*, **49**, 17–27.

Bosi, F. (2013) Bond-valence constraints around the O1 site of tourmaline. *Mineralogical Magazine*, **77**, 343–351.

Bosi, F. and Andreozzi, G.B. (2013) A critical comment on Ertl *et al*. (2012) "Limitations of Fe^{2+} and Mn^{2+} site occupancy in tourmaline: Evidence from Fe^{2+}- and Mn^{2+}-rich tourmaline". *American Mineralogist*, **98**, 2183–2192.

Bosi, F. and Lucchesi, S. (2007) Crystal chemical relationships in the tourmaline group: structural constraints on chemical variability. *American Mineralogist*, **92**, 1054–1063.

Bosi, F. and Skogby, H. (2013) Oxy-dravite, $Na(Al_2Mg)(Al_5Mg)(Si_6O_{18})(BO_3)_3(OH)_3O$, a new mineral species of the tourmaline supergroup. *American Mineralogist*, **98**, 1442–1448.

Bosi, F., Agrosì, G., Lucchesi, S., Melchiorre, G. and Scandale, E. (2005) Mn-tourmaline from island of Elba (Italy): Crystal chemistry. *American Mineralogist*, **90**, 1661–1668.

Bosi, F., Balić-Žunić, T. and Surour, A.A. (2010) Crystal structure analysis of four tourmalines from the Cleopatra's Mines (Egypt) and Jabal Zalm (Saudi Arabia), and the role of Al in the tourmaline group. *American Mineralogist*, **95**, 510–518.

Bosi, F., Reznitskii, L. and Skogby, H. (2012*a*) Oxy-chromium-dravite, $NaCr_3(Cr_4Mg_2)(Si_6O_{18})(BO_3)_3(OH)_3O$, a new mineral species of the tourmaline supergroup. *American Mineralogist*, **97**, 2024–2030.

Bosi, F., Skogby, H., Agrosì, G. and Scandale, E. (2012*b*) Tsilaisite, $NaMn_3Al_6(Si_6O_{18})(BO_3)_3(OH)_3OH$, a new mineral species of the tourmaline supergroup from Grotta d'Oggi, San Pietro in Campo, island of Elba, Italy. *American Mineralogist*, **97**, 989–994.

Bosi, F., Andreozzi, G.B., Agrosì, G. and Scandale, E. (2012*c*) Fluor-tsilaisite, IMA 2012-044. CNMNC Newsletter No. 14, October 2012, page 1287; *Mineralogical Magazine*, **76**, 1281–1288.

Bosi, F., Skogby, H., Hålenius, U. and Reznitskii, L. (2013*a*) Crystallographic and spectroscopic characterization of Fe-bearing chromo-alumino-povondraite and its relations with oxy-chromium-dravite and oxy-dravite. *American Mineralogist*, **98**, 1557–1564.

Bosi, F., Reznitskii, L. and Sklyarov, E.V. (2013*b*) Oxy-vanadium-dravite, $NaV_3(V_4Mg_2)(Si_6O_{18})(BO_3)_3(OH)_3O$: crystal structure and redefinition of the "vanadium-dravite" tourmaline. *American Mineralogist*, **98**, 501–505.

Bosi, F., Andreozzi, G.B., Skogby, H., Lussier, A.J., Abdu, Y. and Hawthorne, F.C. (2013*c*) Fluor-elbaite, $Na(Li_{1.5}Al_{1.5})Al_6(Si_6O_{18})(BO_3)_3(OH)_3F$, a new mineral species of the tourmaline supergroup. *American Mineralogist*, **98**, 297–303.

Bosi, F., Skogby, H., Reznitskii, L. and Hålenius, U. (2014*a*) Vanadio-oxy-dravite, $NaV_3(Al_4Mg_2)(Si_6O_{18})(BO_3)_3(OH)_3O$, a new mineral species of the tourmaline supergroup. *American Mineralogist*, **99**, 218–224.

Bosi, F., Reznitskii, L., Skogby, H. and Hålenius, U. (2014*b*) Vanadio-oxy-chromium-dravite, $NaV_3(Cr_4Mg_2)(Si_6O_{18})(BO_3)_3(OH)_3O$, a new mineral species of the tourmaline supergroup. *American Mineralogist*, **99**, 1155–1162.

Brown, I.D. and Altermatt, D. (1985) Bond-valence parameters obtained from a systematic analysis of the Inorganic Crystal Structure Database. *Acta Crystallographica*, **B41**, 244–247.

Burns, P.C., MacDonald, D.J. and Hawthorne, F.C. (1994) The crystal chemistry of manganese-bearing elbaite. *The Canadian Mineralogist*, **32**, 31–41.

Clark, C.M., Hawthorne, F.C. and Ottolini, L. (2011) Fluor-dravite, $NaMg_3Al_6Si_6O_{18}(BO_3)_3(OH)_3F$, a new mineral species of the tourmaline group from the Crabtree emerald mine, Mitchell County, North Carolina: description and crystal structure. *The Canadian Mineralogist*, **49**, 57–62.

Ertl, A., Hughes, J.M., Prowatke, S., Rossman, G.R., London, D. and Fritz, E.A. (2003) Mn-rich tourmaline from Austria: structure, chemistry, optical spectra, and relations to synthetic solid solutions. *American Mineralogist*, **88**, 1369–1376.

Ertl, A., Kolitsch, U., Darby Dyar, M., Meyer, H.-P., Henry, D.J., Rossman, G.R., Prem, M., Ludwig, T., Nasdala, L., Lengauer, C.L. and Tillmanns, E. (2011) Fluor-schorl, IMA 2010-067. CNMNC Newsletter No. 8, April 2011, page 291; *Mineralogical Magazine*, **75**, 289–294.

Ertl, A., Kolitsch, U., Dyar, M.D., Hughes, J.M., Rossman, G.R., Pieczka, A., Henry, D.J., Pezzotta,

F., Prowatke, S., Lengauer, C.L., Körner, W., Brandstatter, F., Francis, C.A., Prem, M. and Tillmans, E. (2012) Limitations of Fe^{2+} and Mn^{2+} site occupancy in tourmaline: evidence from Fe^{2+}- and Mn^{2+}-rich tourmaline. *American Mineralogist*, **97**, 1402–1416.

Filip, J., Bosi, F., Novák, M., Skogby, H., Tuček, J., Čuda, J. and Wildner, M. (2012) Redox processes of iron in the tourmaline structure: example of the high-temperature treatment of Fe^{3+}-rich schorl. *Geochimica et Cosmochimica Acta*, **86**, 239–256.

Foit, F.F., Jr. (1989) Crystal chemistry of alkali-deficient schorl and tourmaline structural relationships. *American Mineralogist*, **74**, 422–431.

Grice, J.D. and Ercit, T.S. (1993) Ordering of Fe and Mg in the tourmaline crystal structure: the correct formula. *Neues Jahrbuch für Mineralogie, Abhandlungen*, **165**, 245–266.

Hawthorne, F.C. (1996) Structural mechanisms for light-element variations in tourmaline. *The Canadian Mineralogist*, **34**, 123–132.

Hawthorne, F.C. (2002) Bond-valence constraints on the chemical composition of tourmaline. *The Canadian Mineralogist*, **40**, 789–797.

Hawthorne, F.C. and Henry, D. (1999) Classification of the minerals of the tourmaline group. *European Journal of Mineralogy*, **11**, 201–215.

Henry, D.J. and Dutrow, B.L. (2011) The incorporation of fluorine in tourmaline: Internal crystallographic controls or external environmental influences? *The Canadian Mineralogist*, **49**, 41–56.

Henry, D.J., Novák, M., Hawthorne, F.C., Ertl, A., Dutrow, B., Uher, P. and Pezzotta, F. (2011) Nomenclature of the tourmaline supergroup minerals. *American Mineralogist*, **96**, 895–913.

London, D. (2011) Experimental synthesis and stability of tourmaline: a historical perspective. *The Canadian Mineralogist*, **49**, 117–136.

Lussier, A.J., Aguiar, P.M., Michaelis, V.K., Kroeker, S., Herwig, S., Abdu, Y. and Hawthorne, F.C. (2008) Mushroom elbaite from the Kat Chay mine, Momeik, near Mogok, Myanmar: I. Crystal chemistry by SREF, EMPA, MAS NMR and Mössbauer spectroscopy. *Mineralogical Magazine*, **72**, 747–761.

Lussier, A.J., Abdu, Y. Hawthorne, F.C., Michaelis, V.K., Aguiar, P.M. and Kroeker, S. (2011*a*) Oscillatory zoned liddicoatite from Anjanabonoina, central Madagascar. I. Crystal chemistry and structure by SREF and ^{11}B and ^{27}Al MAS NMR spectroscopy. *The Canadian Mineralogist*, **49**, 63–88.

Lussier, A.J., Hawthorne, F.C., Aguiar, P.M., Michaelis, V.K. and Kroeker, S. (2011*b*) Elbaite-liddicoatite from Black Rapids glacier, Alaska. *Periodico di Mineralogia*, **80**, 57–73.

MacDonald, D.J. and Hawthorne, F.C. (1995) The crystal chemistry of Si = Al substitution in tourmaline. *The Canadian Mineralogist*, **33**, 849–858.

Mandarino, J.A. (1981) The Gladstone-Dale relationship. Part IV: the compatibility concept and its application. *The Canadian Mineralogist*, **19**, 441–450.

Nishio-Hamane, D., Minakawa, T., Yamaura, J., Oyama, T., Ohnishi, M. and Shimobayashi, N. (2013) Adachiite, IMA 2012-101. CNMNC Newsletter No. 16, August 2013, page 2700; *Mineralogical Magazine*, **77**, 2695–2709.

Nishio-Hamane, D., Minakawa, T., Yamaura, J., Oyama, T., Ohnishi, M. and Shimobayashi, N. (2014) Adachiite, a Si-poor member of the tourmaline supergroup from the Kiura mine, Oita Prefecture, Japan. *Journal of Mineralogical and Petrological Sciences*, **109**, 74–78.

Novák, M., Škoda, P., Filip, J., Macek, I. and Vaculovič, T. (2011) Compositional trends in tourmaline from intragranitic NYF pegmatites of the Třebíč Pluton, Czech Republic; electron microprobe, Mössbauer and LA-ICP-MS study. *The Canadian Mineralogist*, **49**, 359–380.

Novák, M., Ertl, A., Povondra, P., Galiová, M.V., Rossman, G.R., Pristacz, H., Prem, M., Giester, G., Gadas, P. and Škoda, R. (2013) Darrellhenryite, $Na(LiAl_2)Al_6(BO_3)_3Si_6O_{18}(OH)_3O$, a new mineral from the tourmaline supergroup. *American Mineralogist*, **98**, 1886–1892.

Pouchou, J.L. and Pichoir, F. (1991) Quantitative analysis of homogeneous or stratified microvolumes applying the model "*PAP*." Pp. 31–75 in: *Electron Probe Quantitation* (K.F.J. Heinrich and D.E. Newbury, editors). Plenum Press, New York.

Reznitskii, L., Clark, C.M., Hawthorne, F.C., Grice, J.D., Skogby, H., Hålenius, U. and Bosi, F. (2014) Chromo-alumino-povondraite, $NaCr_3(Al_4Mg_2)(Si_6O_{18})(BO_3)_3(OH)_3O$, a new mineral species of the tourmaline supergroup. *American Mineralogist*, **99**, 1767–1773.

Rossman, G.R. and Mattson, S.M. (1986) Yellow, Mn-rich elbaite with Mn–Ti intervalence charge transfer. *American Mineralogist*, **71**, 599–602.

Sheldrick, G.M. (2013) *SHELXL2013*. University of Göttingen, Germany.

Skogby, H., Bosi, F. and Lazor, P. (2012) Short-range order in tourmaline: a vibrational spectroscopic approach to elbaite. *Physics and Chemistry of Minerals*, **39**, 811–816.

Wright, S.E., Foley, J.A. and Hughes, J.M. (2000) Optimization of site occupancies in minerals using quadratic programming. *American Mineralogist*, **85**, 524–531.